SISSA

PAPER • OPEN ACCESS

Design of a compact Thomson Parabola Spectrometer for diagnostics of proton-boron fusion reaction products initiated by laser

To cite this article: A. Kurmanova *et al* 2023 *JINST* **18** C06027

View the article online for updates and enhancements.

2ND INTERNATIONAL WORKSHOP ON PROTON-BORON FUSION
CATANIA, ITALY
5–8 SEPTEMBER 2022

Design of a compact Thomson Parabola Spectrometer for diagnostics of proton-boron fusion reaction products initiated by laser

A. Kurmanova,[a,b,*] **G. Petringa,**[b,c] **R. Catalano**[b] **and G.A.P. Cirrone**[b,c,d]

[a]*Dipartimento di Fisica e Astronomia "Ettore Majorana", Università di Catania,*
Via S. Sofia 64, Catania, Italy

[b]*INFN-LNS,*
Via S. Sofia 62, Catania, Italy

[c]*ELI Beamlines,*
Za Radnicí 835, 252 41, Dolní Břežany, Czech Republic

[d]*Centro Siciliano di Fisica Nucleare e Struttura della Materia,*
Viale A. Doria 6, Catania, Italy

E-mail: kurmanova@lns.infn.it

ABSTRACT: The proton-boron aneutronic fusion reaction has numerous potential applications varying from controlled nuclear fusion reactor to broad-energy spectrum α-particle source, as well as uses in medicine, where it can serve as a source for radioisotope production, or directly in proton boron capture therapy. However, proton-boron fusion reaction and its by-products should be investigated extensively to provide a stable and controlled secondary ion source. In order to monitor the multi-ion beam emitted and accelerated from the target surface after interaction with laser pulses, a new Thomson Parabola Spectrometer (TPS) has been designed to differentiate proton and alpha traces in the energy ranges 0.5–5 MeV and 1–10 MeV respectively, with a high energy resolution ($\leq 1\%$), while maintaining compactness of the spectrometer (~ 20 cm).

---

*Corresponding author.

Contents

1 Introduction

Developing viable alternatives to nuclear fission has been at the forefront of scientific endeavour for the past few decades. One of the most promising candidates is nuclear fusion, in which the lightest ions — deuterium and tritium (D-T) — collide at high enough energy to overcome the Coulomb barrier and eventually fuse. An alternative to D-T fusion is the aneutronic ^{11}B(p,3α) (proton-boron) fusion reaction [1] which produces three α particles through the following reaction channels [2]:

$$p + {}^{11}_{5}\text{B} \rightarrow \alpha_0 + {}^{8}_{4}\text{Be} + 8.59\,\text{MeV} \rightarrow \alpha_0 + \alpha_{01} + \alpha_{02} + 8.59\,\text{MeV} \tag{1.1}$$

$$p + {}^{11}_{5}\text{B} \rightarrow \alpha_1 + {}^{8}_{4}\text{Be}^* + 5.65\,\text{MeV} \rightarrow \alpha_1 + \alpha_{11} + \alpha_{12} + 5.65\,\text{MeV} \tag{1.2}$$

$$p + {}^{11}_{5}\text{B} \rightarrow 3\alpha + 8.68\,\text{MeV} \tag{1.3}$$
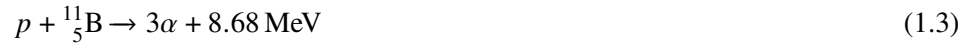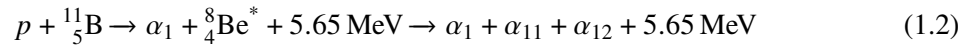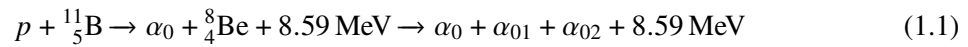
The reaction can proceed in a single step and produce three α particles shown in the reaction channel (1.3), but it contributes less than 5% to the total overall process. In the dominant reaction channels (1.1) and (1.2), formation of the excited state ${}^{8}_{4}\text{Be}^*$ occurs, followed by its decay into two secondary α particles with a continuous energy spectrum. As a result of the above reactions, the spectrum of alpha particles ranges from a few hundred keV up to 10 MeV with a peak around 4 MeV [2].

Although the proton-boron reaction has a lower gain factor and requires higher energy compared to its D-T counterpart, it has obvious advantages such as direct energy conversion and a smaller number of neutrons [3]. In addition, the proton-boron reaction is considered as a powerful alpha source, making it an important contributor to radioisotope production [4]. Although the benefits are numerous, the reaction needs to be studied in detail to make it controllable for future applications. To study the reaction mechanisms and its products in detail, diagnostic tools and techniques must be handy and function under intense operating conditions. Some examples of such detection systems are time-of-flight (ToF) detectors, nuclear track detectors, and Thomson Parabola Spectrometers (TPS). The latter detector is capable of resolving both the type and energy of ions and was therefore chosen as the basis for our research. In this work, we report a new TPS design developed to distinguish

proton and α tracks in 0.5–5 MeV and 1–10 MeV respectively, corresponding to the realistic energy ranges reported in experiments [2]. The new design will provide high energy resolution ($\leq 1\%$) and compactness in the experimental setup (about 20 cm), taking into account the limited size of the ion detector. The design was finalised after extensive parameter verification with analytical formulae and validation with realistic beam simulation models such as the Monte Carlo-based toolkit [5] and the Boris solver [6] implemented in Python.

2   Theoretical analysis

A TPS operates using a combination of parallel electric and magnetic fields that resolve ion tracks according to their energy and mass-to-charge ratio (m/q) as determined by the Lorentz force [7]. The generic design consists of a pinhole to collimate the beam, an electric field region, a magnetic field region, and an ion detector. Figure 1 shows the schematic representation of a general TPS, with electric and magnetic fields applied along the positive Y-axis.
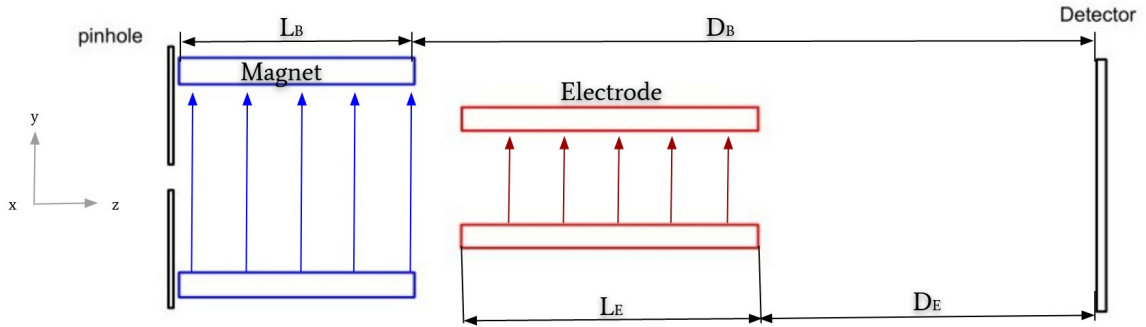

Figure 1. Schematic representation of a typical TPS design with static electric and magnetic fields.

Ions generated by the laser-target interaction move toward the TPS and are collimated by the pinhole. The collimated ions move into the active region of the uniform transversely applied fields and diffuse along the X-axis by virtue of their energy according to eq. (2.1), and simultaneously deflected along the Y-axis on account of their m/q ratio according to eq. (2.2).

$$x = \frac{qB_0L_B}{\sqrt{2mE}}\left(D_B + \frac{L_B}{2}\right) \tag{2.1}$$

$$y = \frac{qE_0L_E}{2E}\left(D_E + \frac{L_E}{2}\right) \tag{2.2}$$

Here q and m are the charge and mass of the ion, B_0, E_0 represent the magnetic and electric field magnitudes, E is the energy of the ions, L_B, L_E are the active lengths of the field along the direction of beam propagation (in this case along the Z-axis), and D_E, D_B are the drift lengths, defined as the distance from the end of the electric and magnetic fields to the ion detector.

One of the reaction by-products are photons which pass through the applied electromagnetic fields of the spectrometer undeflected since they carry no charge. As such, they provide a useful reference point on the detector with respect to which the ions deflected by the Lorentz force produce a

parabolic curve described by eq. (2.3), simplified from eqs. (2.1) and (2.2) using some algebraic steps:

$$y = \frac{mE_0 L_E (D_E + \frac{L_E}{2})}{q B_0^2 L_B{}^2 (D_B + \frac{L_B}{2})^2} x^2 \qquad (2.3)$$

Thus, it is clear that the parabolic tracks on the detector can be distinguished according to the ions' m/q ratio and energy E, by tuning the applied field strengths and their lengths. Optimising these parameters requires quantifying their impact on the spectrometer's performance, through the use of certain physical indicators. The magnetic field, for example, is responsible for dissipating particles according to their energy and thus energy resolution can be taken as a suitable indicator to assess/optimise the magnetic field strength and its active length. The energy resolution is limited by the size of the pinhole δR and is defined by the relation $\delta E = (dE/dR)\delta R$, where R is the displacement of the ion from the reference point. The displacement is defined by $R = \sqrt{x^2 + y^2}$, where x and y are values obtained from eq. (2.1) and (2.2). Using the above equations, the energy resolution is expressed as follows (see [8])

$$\frac{\delta E}{E} = \frac{2E\delta R}{\sqrt{4b^2 + a^2 E}} \qquad (2.4)$$

where a and b are defined as $x(E) = a/\sqrt{E}$ and $y(E) = b/E$.

Using eq. (2.4), the energy resolution was calculated by varying the combination of magnetic field parameters and some results are reported in table 1. Figure 2 shows the variation trends in the energy resolution on changing B_0 — it can be noticed that higher fields generally lead to better (lower) resolution. The analysis has been performed using protons and not α particles, as is commonly done.

Table 1. Energy resolution of protons obtained by varying magnetic field parameters. The finalised parameters are shown in the last row.

L_B, cm	D_B, cm	B_0, T	Energy resolution, %
5	0	0.1	74.15
10	1	0.1	12.12
15	3	0.2	1.93
12	7	0.4	1.03

After analysing the impact of magnetic field properties and taking into account the objective of developing a compact yet high resolution spectrometer ($\leq 1\%$) for the given proton energy range, a high magnetic field of $B_0 = 0.4$ T with a length of $L_B = 12$ cm and a pole separation of 3 cm was chosen to maximise the energy resolution analytically.

Towards the reference point, the tracks of the high-energy ions start to merge, which complicates the discrimination process. To avoid this merging and improve the spatial resolution, the electric field parameters can be adjusted to increase the distance between adjacent ion tracks. Just as with the magnetic field, the effect of the electric field was studied by using spatial resolution as an indicator
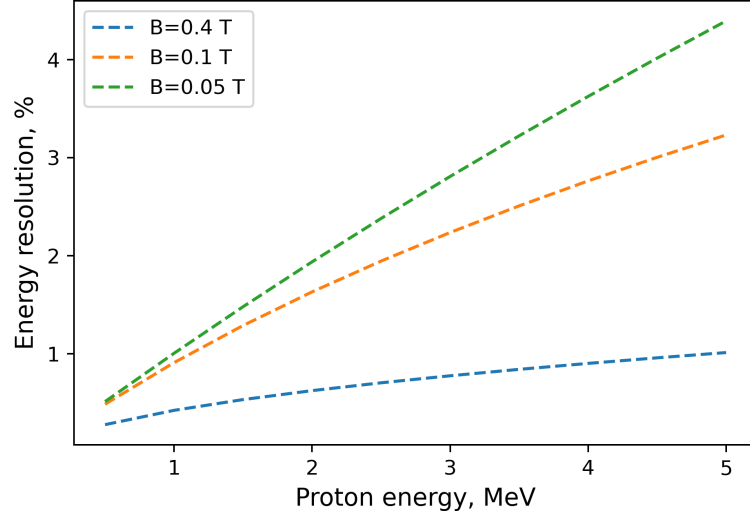
Figure 2. Comparison of proton energy resolution obtained with permanent magnets plates of dimension $120 \times 77\,\text{mm}^2$ for $B_0 = 0.05\,\text{T}$, $B = 0.1\,\text{T}$ and $B_0 = 0.4\,\text{T}$, assuming $D_B = 70\,\text{mm}$.

of sufficient (approximate) separation, given by the expression (see in [9]):

$$\delta = \left| \frac{y_2 - y_1}{s} \right|_{x_1 = x_2} = \frac{Z_1}{A_1} \frac{E_0 L_E (D_E + 0.5 L_E)}{sc^2} \frac{\gamma_1}{\gamma_1^2 - 1} \left| 1 - \frac{1}{\gamma_1} \sqrt{\gamma_1^2 - 1 + \left(\frac{Z_1}{Z_2} \frac{A_2}{A_1} \right)^2} \right| \qquad (2.5)$$

where y_1 and y_2 stand for the electric field displacements of two ion species with atomic numbers Z_1 and Z_2 and mass numbers A_1, A_2; γ_1 is the Lorentz factor, c is the speed of light and s stands for the diameter of the pinhole defining the width of the ion track on the detector plane.

Using eq. (2.5) and varying parameters such as length and applied voltage, the changes in spatial resolution were analysed. Some results of the parameter sweep are shown in the table 2 and the changes due to the applied voltage in figure 3. Since the drift length directly affects the size of the parabola on the detector plane (which has a finite area) it was necessary to keep it small and hence $D_B = D_E$ was fixed to the finalised value of 7 cm as shown in table 1.

Table 2. Spatial resolution between protons and α particles obtained by varying electric field parameters. D_E fixed for all combinations.

L_E, cm	E_0, MV/m	Spatial resolution, cm
5	1.0	0.04
7	1.8	0.13
8	2.0	0.17
9	1.85	0.19

Figure 3 shows an increase in spatial resolution on using higher electric fields. Consequently, the field was set to $E_0 = 1.85\,\text{MV/m}$ with $L_E = 9\,\text{cm}$ to finalise the design. The compactness of the spectrometer was maintained by completely overlapping the electric and magnetic fields, as shown in the finalised schematic of figure 4.
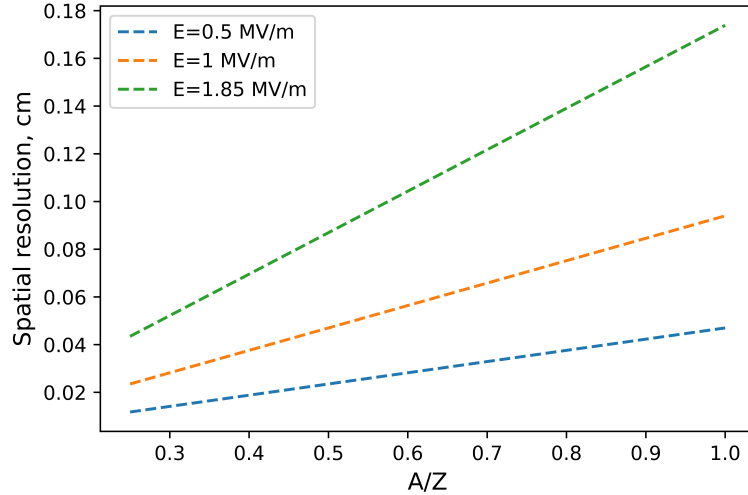
Figure 3. Comparison of spatial resolution between proton and α tracks achieved with electrode plates of dimensions 90×77 mm^2 at $E_0 = 0.5$ MV/m, $E_0 = 1$ MV/m and $E_0 = 1.85$ MV/m, assuming $D_E = 70$ mm.
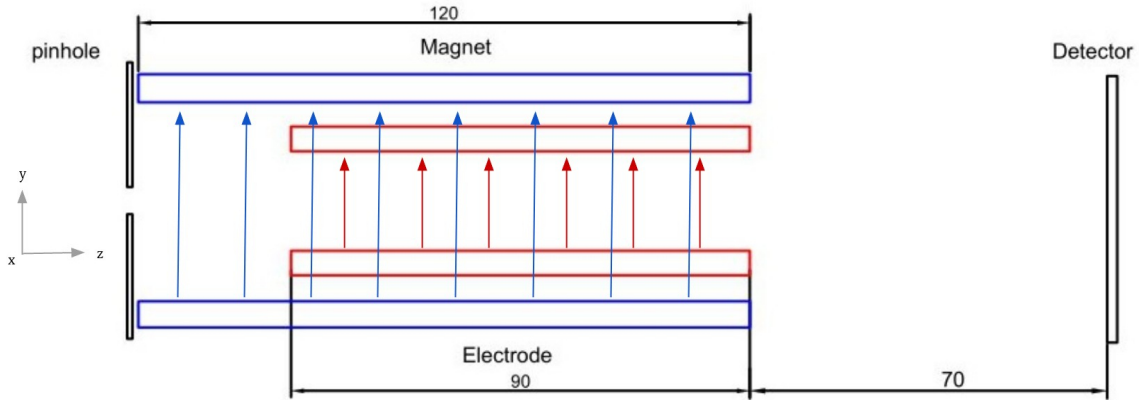

Figure 4. Schematic representation of a TPS design defined analytically (all lengths in mm).

3 Modelling

Once a preliminary idea of the spectrometer design parameters were obtained using analytical formulae, the expected outcome of the experiment was simulated to evaluate the effect of random sampling and realistic ion beams. For this reason, the design of the spectrometer was modelled using two approaches — a Monte Carlo based simulation toolkit Topas [5], and a self-developed beam transport code based on the Boris algorithm [6] in Python.

Topas. Topas (TOol for PArticle Simulation), based on a Geant4 simulation tool, is considered a reliable and experimentally validated simulation tool [5] that models particle transport numerically using a standard Runge-Kutta based differential equation solver.

A 3D model of the TPS design schematics as shown in figure 4 was generated and simulated in Topas. A beam containing protons was defined as a point source at a distance of 3 cm from the collimator energies sampled from a discrete, uniform distribution in the range [0.5 MeV, 5 MeV]

in 10 bins. The beam divergence was kept low for simplicity ($\sim 0.1°$). The magnetic and electric fields were considered to be uniform, and the detector plane was placed perpendicular to the beam direction at a distance $D_E = D_B = 7$ cm from the electric plates. The 2D image of the proton trace in a parabolic shape was obtained from the Topas simulation and is shown in figure 5.
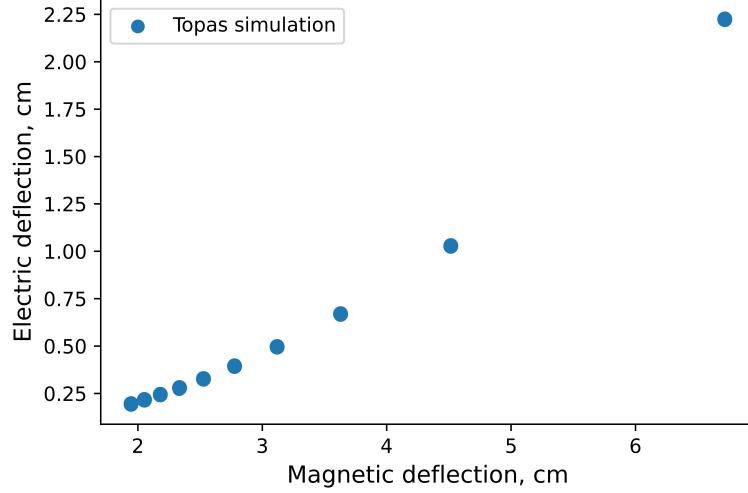

Figure 5. Proton position on the detector as simulated by Topas.

Boris method. Numerical modelling of ion transport in the electromagnetic field was also performed using the Boris algorithm. This algorithm is a second order accurate leapfrog scheme and uses a time staggered discretization for the velocity and the position of the particle, such that the position at a half time step ($x^{n+1/2}$) is used to define the velocity of the particle centred on integer time steps (v^n), and the calculated velocity at an integer time step is used to define the position at a half time step [6].

The motion of a charged particle in electromagnetic fields **E** and **B** has the following discrete form:

$$\frac{x^{n+\frac{1}{2}} - x^{n-\frac{1}{2}}}{\Delta t} = \frac{u^n}{\gamma^n} \tag{3.1}$$

$$m\frac{u^{n+1} - u^n}{\Delta t} = q\left(E^{n+\frac{1}{2}} + \bar{v}^{n+\frac{1}{2}} \times B^{n+\frac{1}{2}}\right) \tag{3.2}$$

where $(n, n+1, \ldots)$ indicates time steps, $u = \gamma v$ is the relativistic momentum vector, Δt is the discrete time step and $\bar{v}^{n+1/2}$ is the effective velocity.

The particle motion is divided into three parts: two parts are devoted to the electric field in the first (3.3) and second half-step (3.5), while the rotation section is considered for the whole time step (3.4).

$$u^- = u^n + \frac{q\Delta t}{2m}E^{n+\frac{1}{2}} \tag{3.3}$$

$$\frac{u^+ - u^-}{\Delta t} = \frac{q}{m}\left(\bar{v}^{n+\frac{1}{2}} \times B^{n+\frac{1}{2}}\right) \tag{3.4}$$

$$u^{n+1} = u^+ + \frac{q\Delta t}{2m}E^{n+\frac{1}{2}} \tag{3.5}$$

The Boris approach was implemented in Python to determine the final position of the proton on the detector plane, and differed from the Topas implementation in that the Runge-Kutta differential solver was replaced by a more adept charge transport model. A beam of $N = 10^5$ protons was sampled from the same energy interval as used in Topas and randomly distributed in the flat, circular profile. To model the discretized ion transport, the time step was calculated as a small percentage ($\sim 10\%$) of the ratio between the active length of the fields and the initial particle velocity. After verifying the beam passage through the collimator, the protons were moved into the active region of the magnetic field, where the position and velocity were estimated by rotation using the eq. (3.4) at each time step. Crossing the pure magnetic field, the beam entered into the active electric plus magnetic field zone and the proton positions were updated according to eq. (3.3), (3.5) and eq. (3.4). The beam exiting the field region continued to move according to the evolved velocities towards the detector plane, and the impinging protons created the parabolic trace shown in figure 6.
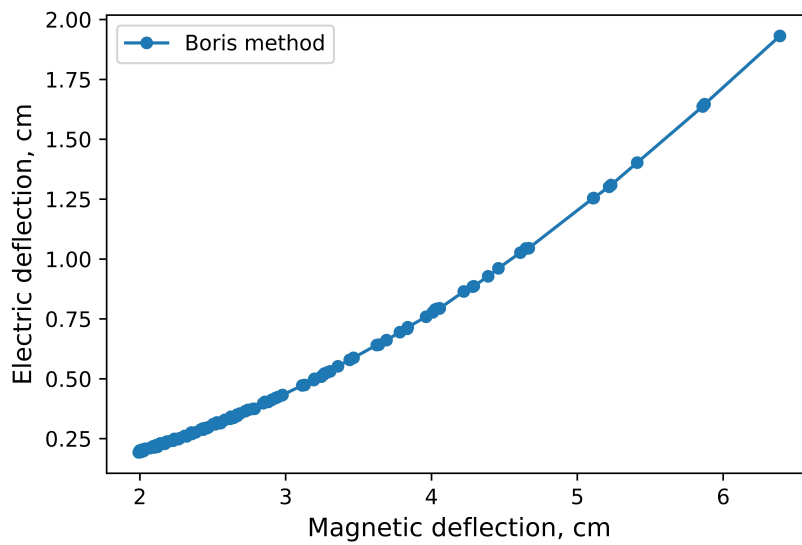

Figure 6. Proton position on the detector as simulated by Boris method.

4 Discussion

To meet the requirements of a TPS intended for low energy particle detection, it was important to enhance the energy resolution, which was found to improve upon using a high strength magnetic field and a long magnet. Therefore, the TPS with the magnet with $L_B = 12$ cm, $B_0 = 0.4$ T and $D_B = 7$ cm should provide a well resolved energy spectrum that can be registered with 1% energy resolution for protons up to 5 MeV. The spatial resolution of high energy particles was increased to ~ 0.2 cm by using a strong electric field (up to the vacuum breakdown voltage) $E_0 = 1.85 \, MV/m$ and $L_E = 9$ cm while keeping the drift range constant. And finally, by overlapping the magnet and the electrode, the overall size of the TPS was constrained to about 20 cm, which allows it to be placed inside the target-laser chamber. This is very important because the proton-boron fusion reaction produces a low alpha flux and the spectrometer must be placed in close proximity.

To verify the design two models simulated in different tools and using different approaches Topas simulation and Boris method were utilized and the comparison between three methods are shown in figure 7. All three parabolic traces show an overall match and predict $\leq 1\%$ energy resolution. There are some discrepancies for low energy protons which can be explained in different ways. The deviation in the analytical curve naturally arises due to its inability to capture the added horizontal velocity imparted by the $B_0 = 0.4\,\text{T}$ magnetic field. This difference vanishes on using a low $B_0 = 0.1\,\text{T}$ field per expectations. The mismatch between Topas and Boris results for low energy protons may instead be explained by lower accuracy in the differential solver employed by the former, but requires more comprehensive analysis. Either way, the importance of simulations in finalising design parameters is evident when using high magnetic fields.
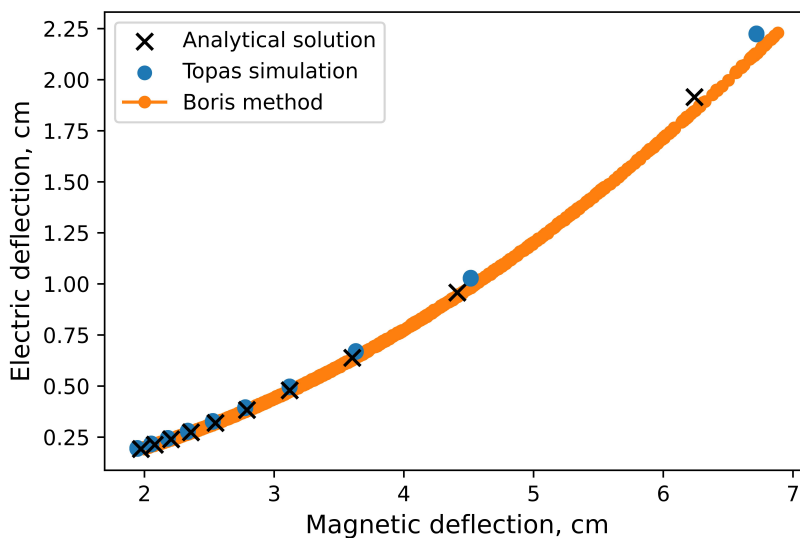

Figure 7. Comparison between proton position curves on the detector plane as calculated analytically, simulated with Topas toolkit and calculated using Boris approach.

5 Conclusion

The design of TPS, which can provide high energy resolution ($\leq 1\%$) and adequate spatial resolution ($\approx 0.2\,\text{cm}$) to distinguish the protons and α-particles produced as products of the proton-boron fusion reaction, has been demonstrated. The TPS will be assembled in the near future and the results will be compared with analytical and model solutions.

References

[1] D.C. Moreau, *Potentiality of the proton-boron fuel for controlled thermonuclear fusion*, *Nucl. Fusion* **17** (1977) 13.

[2] C. Labaune et al., *Laser-initiated primary and secondary nuclear reactions in Boron-Nitride*, *Sci. Rep.* **6** (2016) 21202.

[3] G.A. Ruggiero, *Proton boron colliding beams for nuclear fusion*, No. BNL-67212; KA040301, Brookhaven National Lab. (BNL), Upton, NY, U.S.A. (2000).

[4] S.M. Qaim, I. Spahn, B. Scholten and B. Neumaier, *Uses of alpha particles, especially in nuclear reaction studies and medical radionuclide production*, *Radiochim. Acta* **104** (2016) 601.

[5] B. Faddegon et al., *The TOPAS tool for particle simulation, a monte carlo simulation tool for physics, biology and clinical research*, *Phys. Med.* **72** (2020) 114.

[6] S. Zenitani and T. Umeda, *On the Boris solver in particle-in-cell simulation*, *Phys. Plasmas* **25** (2018) 112110 [arXiv:1809.04378].

[7] J.J. Thomson, *XXVI. Rays of positive electricity*, *Philos. Mag.* **21** (1911) 225.

[8] S. Kojima et al., *Compact Thomson parabola spectrometer with variability of energy range and measurability of angular distribution for low-energy laser-driven accelerated ions*, *Rev. Sci. Instrum.* **91** (2020) 053305.

[9] A. Alejo et al., *Recent developments in the Thomson Parabola Spectrometer diagnostic for laser-driven multi-species ion sources*, 2016 *JINST* **11** C10005.